Simulation Study of Al Channeling in 4H-SiC

Hobler, Gerhard

IEEE
2018

Hobler , G , Nordlund , K , Current , M & Schustereder , W 2018 , Simulation Study of Al Channeling in 4H-SiC . in V Häublein & H Ryssel (eds) , IIT 2018 Proceedings . IEEE , pp. 247-250 , International Conference on Ion Implantation Technology , Würzburg , Germany , 16/09/2018 .

http://hdl.handle.net/10138/308763

2018 22nd International Conference on Ion Implantation Technology

September 16-21, 2018

Congress Centrum, Würzburg, Germany

IIT 2018 Proceedings

Editors

Volker Häublein

Heiner Ryssel

IEEE

ELECTRON DEVICES SOCIETY

Simulation Study of Al Channeling in 4H-SiC

Gerhard Hobler
Institute of Solid-State Electronics
TU Wien
Vienna, Austria
gerhard.hobler@tuwien.ac.at

Kai Nordlund
Department of Physics
University of Helsinki
Helsinki, Finland
kai.nordlund@helsinki.fi

Michael Current
Current Scientific
San Jose, USA
currentsci@aol.com

Werner Schustereder
Infineon Technologies Austria AG
Villach, Austria
werner.schustereder@infineon.com

***Abstract*—The modeling of channeled Al implantation into SiC in a Monte Carlo binary collision (BC) framework is revisited, using experimental data from 60 keV to 1.5 MeV in a dose range from 1.8×10^{12} to 4.1×10^{14} Al/cm^2. From simulated channeling maps, [0001], [11$\bar{2}$3], and [11$\bar{2}$0] are determined as the three major channeling directions in 4H-SiC. 1D and 2D implant distributions are investigated. It is found that implantation in channeling directions provides more abrupt profiles with considerably less penetration beneath a mask edge than random implants. Channeling along [11$\bar{2}$0] has a clear advantage over [0001] and [11$\bar{2}$3], both in terms of less lateral penetration and lower sensitivity to implant damage and beam divergence. The validity of the BC simulations is corroborated by molecular dynamics (MD) simulations for selected conditions.**

***Index Terms*—channeling, SiC, Monte Carlo simulation**

I. Introduction

Aluminum is commonly used as a dopant for p-wells of SiC power devices. Channeling leads to tails in the dopant distributions, or it could be used intentionally to produce deeper, more box-like profiles with less tails. In both cases, a better understanding of the channeling characteristics can help in developing process recipes to achieve desired dopant distributions.

SIMS profiling and modeling of ion implantation in SiC has received increased interest in the late 1990s and early 00s of the current century [1]–[5]. With the currently increasing importance of SiC in power electronics and the improved ion implantation machine controls on wafer and beam orientation, wafer temperature and dosimetry, it seems appropriate to revisit the modeling of ion implantation in SiC and to explore the possibilities channeling provides for tailoring the distribution of the implanted ions.

II. Simulation Tools

A. Binary Collision Simulation

Monte Carlo binary collision (BC) simulations are performed with IMSIL [6]. For this study, the ideal 4H- and 6H-SiC lattice structures have been implemented with an atomic density of $N = 9.66 \times 10^{22}$ cm^{-3}. Damage to the crystal structure is taken into account by isolated Frenkel pairs whose concentration is calculated using the modified Kinchin-Pease model with displacement energies of 30 eV for Si atoms and 20 eV for C [7]. A correction factor $f_{\rm rec}$ to the concentrations is used to calibrate the model to experimental data. Lattice vibrations are implemented as Gaussian displacements from the lattice sites according to the Debye model with a Debye temperature of 1120 K [7]. For the interatomic potential the universal ZBL potential [8] is used with a cutoff impact parameter of 2.67 Å. Ion beam divergence is considered, if specified, by a Gaussian distribution of angles with a standard deviation of 0.5°.

Under channeling conditions, electronic stopping is reduced compared to motion in random direction. We use a model composed of a nonlocal and an impact parameter dependent part. The electronic energy loss in a collision is given by

$$\Delta E_{\rm e} = S_{\rm e}\left[x^{\rm nl} N \Delta R + \frac{1-x^{\rm nl}}{2\pi a^2}\exp\left(-\frac{p}{a}\right)\right] \qquad (1)$$

where p denotes the impact parameter and ΔR the length of the preceding free flight path. For the electronic stopping power $S_{\rm e}$ the Lindhard model [9] is used with a correction factor $k_{\rm corr}$. a is expressed as $a = f_{\rm scr} a_{\rm ZBL}/0.3$ with $a_{\rm ZBL}$ the screening length of the ZBL interatomic potential [8]. $k_{\rm corr}$, $x^{\rm nl}$, and $f_{\rm scr}$ are parameters which have to be fitted to experimental data.

B. Molecular Dynamics

Molecular dynamics simulations are performed with MDRANGE [10]. MDRANGE does not follow the recoils once they are outside the interaction range of the ion, and does not consider interaction between target atoms. This makes range simulations of keV and MeV ions possible. As for the BC simulations, the universal ZBL potential [8] is used, here with a cutoff distance of 3 Å, and lattice vibrations are taken into account by the Debye model. All simulations are run without electronic stopping to enable comparison with BC, since electronic stopping is handled differently in BC and MD.

III. Calibration and Testing

A. Calibration of the BC Model

The calibration of the Lindhard correction factor $k_{\rm corr}$ of the electronic stopping model requires dopant profiles for implant energies where electronic stopping dominates. We find $k_{\rm corr} = 1$ to provide a good fit to experimental projected ranges for Al in SiC [4] over a large energy range, in agreement with the literature [5].

For the calibration of the parameters $x^{\rm nl}$ and $f_{\rm scr}$, dopant profiles of ions channeled along different crystallographic directions are required. Such data exist for 60 keV [3]. The

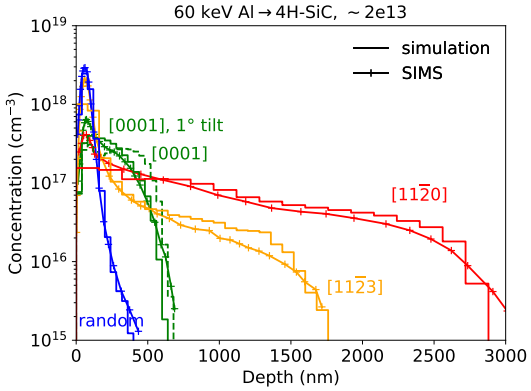

Fig. 1. Comparison of BC results using the calibrated model (histograms) and SIMS results [3] (solid lines with crosses) for $\sim 2 \times 10^{13}$ cm^{-2} 60 keV Al implantations in 4H-SiC in the directions listed in Tab. I.

TABLE I
IMPLANT CONDITIONS FOR DIRECTIONS MENTIONED IN THE TEXT. THE ROTATION ANGLE IS MEASURED FROM THE (01$\bar{1}$0) PLANE.

direction	wafer	tilt	rotation
random	(0001)	9°	0°
[0001]	(0001)	0°	–
[11$\bar{2}$3]	(0001)	17°	0°
[11$\bar{2}$0]	(11$\bar{2}$0)	0°	–

implant conditions used for the fitting are listed in Tab. I (we will refer to these conditions throughout the paper with the names listed in column 1). We find the best fit with $x^{\mathrm{nl}} = 0.07$ and $f_{\mathrm{scr}} = 0.55$. The comparison of the simulations using these parameters with the experimental SIMS profiles is shown in Fig. 1.

To determine the damage recombination factor f_{rec}, implant profiles at increasing doses are required, where damage increasingly blocks the channels. Since we found no useful data for 4H-SiC, we used data for 1.5 MeV Al implanted in [0001]

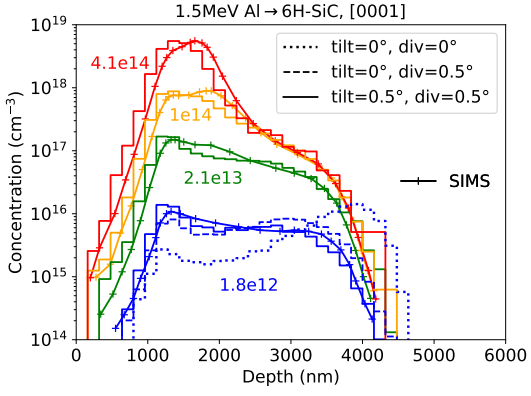

Fig. 2. Comparison of BC results using the calibrated model (histograms) and SIMS results [1] (solid lines with crosses) for 1.5 MeV channeling implantations of Al in the [0001] direction of 6H-SiC. The simulations assume a misalignment of 0.5° and a beam divergence of 0.5° (solid histograms), only a beam divergence of 0.5° (dashed histogram), or ideal conditions (dotted histogram). The labels near the profiles indicate the dose (cm^{-2}).

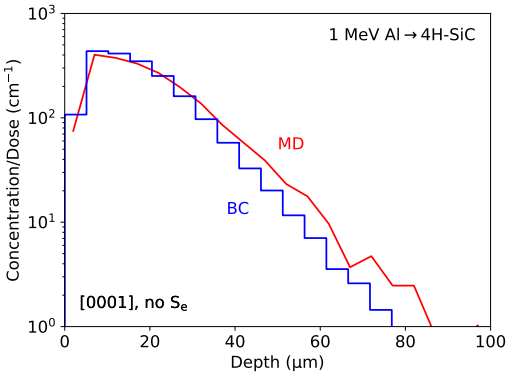

Fig. 3. Comparison of BC (blue histogram) and MD result (red line) for a 1 MeV Al implant channeled along the [0001] direction of 4H-SiC. Electronic stopping has been disregarded.

channeling direction of 6H-SiC to determine $f_{\mathrm{rec}} = 2$, see Fig. 2. The SIMS data could only be fitted by assuming a misalignment and beam divergence of 0.5°.

B. Comparison of BC and MD Results

As a partial test of the BC model we compare a channeling profile in [0001] direction obtained without electronic stopping with results from MDRANGE (Fig. 3). Good agreement is found with slightly underestimated channeling by the BC simulations. Further tests have been performed for the [11$\bar{2}$3] direction and various tilt angles, see Sect. IV-B

IV. RESULTS

A. Channeling Maps

To obtain an overview of channeling directions, the projected range can be plotted as a function of incidence angles (tilt and rotate) in a polar plot. Such a "channeling map" is shown in Fig. 4a for 100 keV Al in (0001)-4H-SiC. Pronounced channeling is visible in the [0001] direction (center) and in six ⟨11$\bar{2}$3⟩ directions (17° from [0001]). Other channeling directions are found at larger tilt angles and along the three {11$\bar{2}$0} planes, although with less pronounced ranges.

A channeling map for 100 keV Al in (11$\bar{2}$0)-4H-SiC is shown in Fig. 4b. The [11$\bar{2}$0] direction is the dominant axial channel, and (0001) is a channeling plane. From these maps it may be concluded that [0001], [11$\bar{2}$3], and [11$\bar{2}$0] are the major channels in 4H-SiC.

B. Channel Characteristics

To characterize the maximum range of the ions, range profiles have been calculated for a dose of 10^{13} cm^{-2}, and the depth where the concentration drops to 10^{15} cm^{-3} has been determined. The results are shown in Fig. 5a. The largest range is obained for channeling along [11$\bar{2}$0], followed by [11$\bar{2}$3], [0001], and the random direction.

For applications the effect of misalignment and beam divergence are important. The sensitivity to these nonideal properties is characterized by the critical angle. To obtain it, we have performed simulations with small increments of tilt

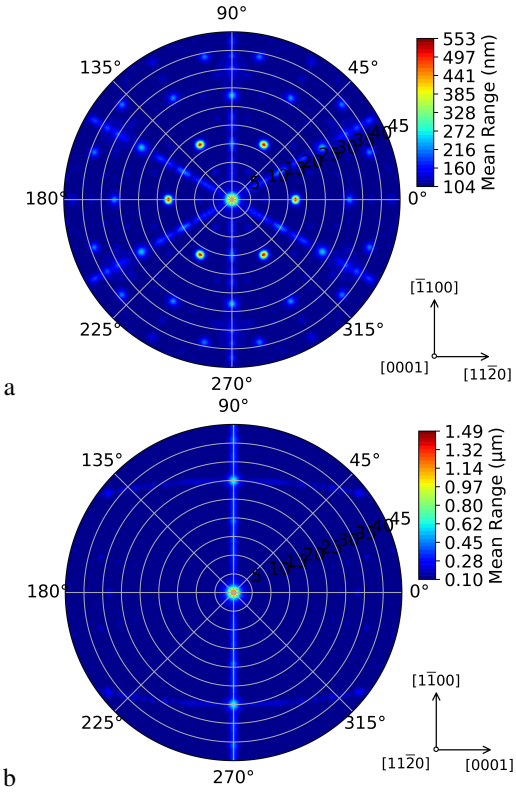

Fig. 4. Channeling maps of 100 keV Al in 4H-SiC for tilt angles of 0° to 45° from the wafer normal and twist angles from 0° to 360°. The color indicates the mean ion range projected to the incidence direction. (a) (0001)-4H-SiC, (b) (11$\bar{2}$0)-4H-SiC.

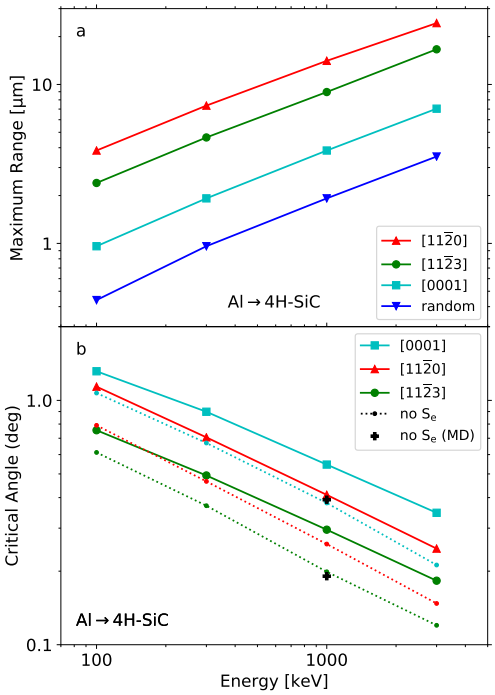

Fig. 5. (a) Maximum range (see text) and (b) critical angle for Al ions channeled along the [0001], [11$\bar{2}$3], and [11$\bar{2}$0] axis of 4H-SiC as a function of implant energy. Solid and dotted lines: Results of BC simulations obtained with and without electronic stopping, respectively. Crosses: MD results. The range data include random implants.

from the nominal direction, and determined the critical angle as the angle yielding a projected range equal to the mean of its value at perfect alignment and its saturation value at large tilt angles. The results for the critical angles are shown in Fig. 5b. Here [0001] is followed by [11$\bar{2}$0] and [11$\bar{2}$3]. Usually, one would expect the reverse order compared to the maximum range. Notably, this is not the case for [11$\bar{2}$0] and [11$\bar{2}$3].

It is interesting to note that the critical angles depend on electronic stopping. The critical angles obtained without consideration of electronic stopping (dotted lines in Fig. 5b) are significantly lower than when electronic stopping is taken into account. For two cases ([0001] and [11$\bar{2}$3], 1 MeV) the critical angles have also been determined by MD (crosses). The agreement with BC is excellent.

C. Dopant Distributions under Ideal Conditions

2D dopant distributions after 1 MeV Al implants near the edge of an impenetrable mask are shown in Fig. 6a for random and the three channeling conditions. In all cases the mask edge and the ion beam direction are parallel to (1$\bar{1}$00). As expected, the penetration depth increases from random to [0001] to [11$\bar{2}$3] to [11$\bar{2}$0]. In addition, the lateral penetration decreases in the same order, in particular at larger depths. Accordingly, the dopant distribution evolves towards a box-like shape.

A comparison of the dopant distributions for implant energies leading to the same maximum range of about 4 µm is shown in Fig. 6b. Here the decrease in lateral penetration from random to [11$\bar{2}$0] is even more pronounced.

D. Dopant Distributions under Nonideal Conditions

In Fig. 6 the effect of implantation damage is already included. In Fig. 7 the corresponding 1D dopant profiles are shown by the solid green lines. For comparison, the simulation results without damage are shown by the dotted blue lines. As can be seen, implantation damage reduces channeling at a dose of 10^{14} cm^{-2}, but only moderately. Also shown in Fig. 7 are the effects of high temperature (not considering the influence of temperature on damage) and beam divergence. All these nonidealities decrease channeling, but leave the essential features of the dopant distributions intact. This is also the case for the 2D distributions, see Fig. 8.

V. Conclusion

Our simulations show that intentional channeling offers the opportunity to produce near-box-like Al profiles in 4H-SiC. Damage formation up to a dose of 10^{14} cm^{-2}, elevated temperatures, and state-of-the art beam divergence are not prohibitive. Channeling along [11$\bar{2}$0] has a clear advantage over [0001] and [11$\bar{2}$3]. Obtaining additional SIMS profiles in order to confirm these predictions as well as for improving model calibration would be worthwhile.

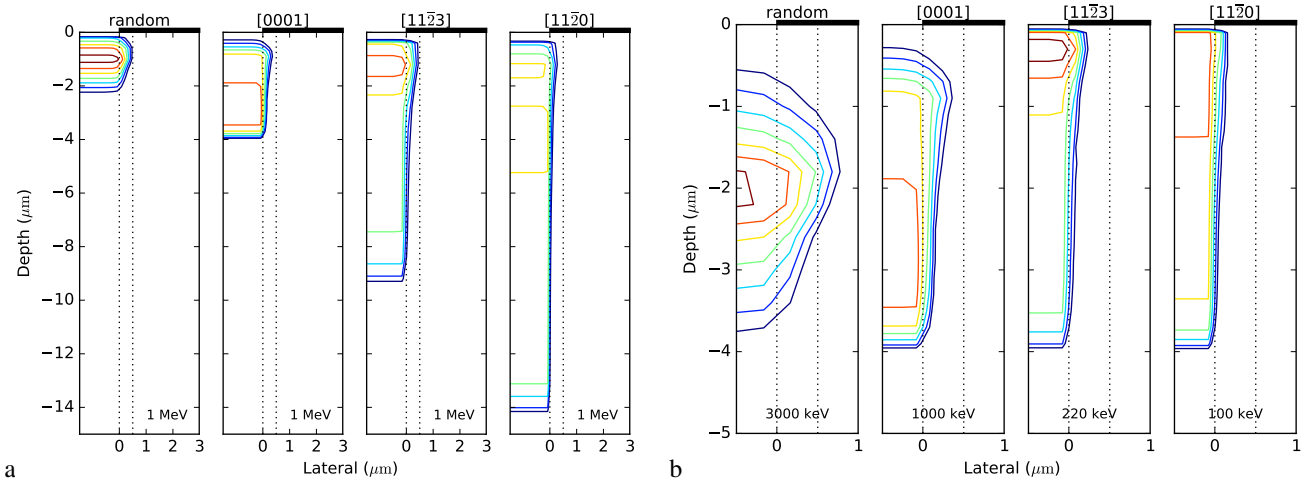

Fig. 6. 2D dopant distributions at an impenetrable mask after implantation of 10^{14} cm^{-2} Al in random direction, along [0001], [11$\bar{2}$3], and [11$\bar{2}$0]). (a) 1 MeV, (b) energy chosen as to obtain a maximum range of about 4 µm. The mask edge is parallel to (1$\bar{1}$00). Two isolines per decade with the lowest level corresponding to 10^{15} cm^{-3}.

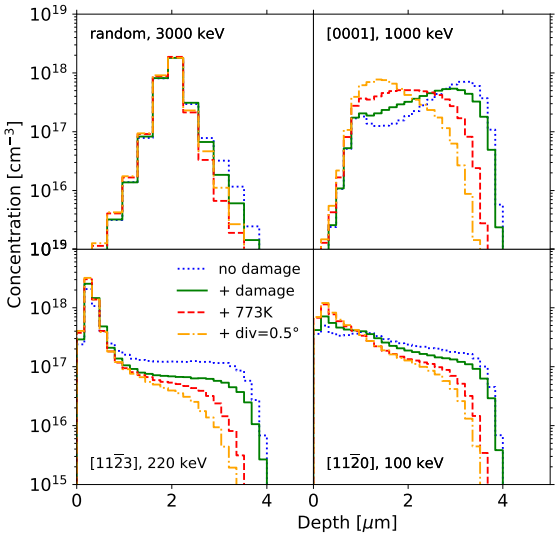

Fig. 7. 1D dopant distributions after implantation of 10^{14} cm^{-2} Al in random direction and three channeling directions. Dotted blue lines: ideal conditions; solid green lines: considering implant damage; dashed red lines: in addition changing the temperature from 300 K to 773 K; dash-dotted yellow lines: in addition considering a beam divergence of 0.5°.

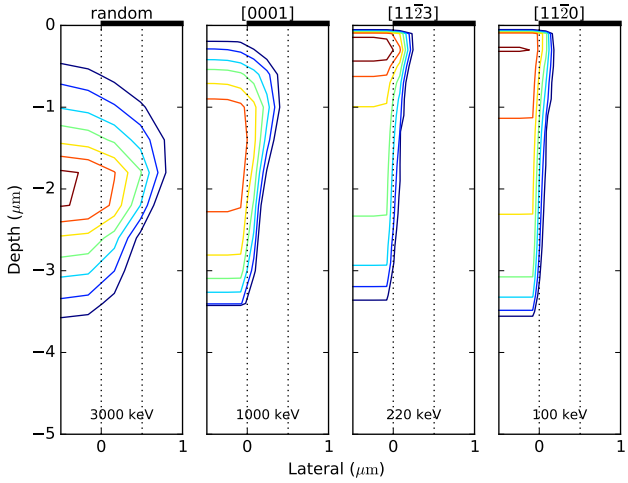

Fig. 8. 2D dopant distributions after high-temperature (773 K) implantation of 10^{14} cm^{-2} Al at an impenetrable mask in random direction and three channeling directions. A beam divergence of 0.5° has been assumed. The mask edge is parallel to (1$\bar{1}$00). Two isolines per decade with the lowest level corresponding to 10^{15} cm^{-3}.

References

[1] E. Morvan, P. Godignon, M. Vellvehi, A. Hallén, M. Linnarsson, and A. Y. Kuznetsov, "Channeling implantations of Al+ into 6H silicon carbide," *Appl. Phys. Lett.*, vol. 74, no. 26, pp. 3990–3992, Jun. 1999.

[2] A. Ster, M. Posselt, A. Hallén, and M. Janson, "Atomistic simulation of ion implantation into different polytypes of SiC," in *Ion Implantation Technology–2000*. IEEE, Piscataway, 2001, pp. 220–223.

[3] J. Wong-Leung, M. S. Janson, and B. G. Svensson, "Effect of crystal orientation on the implant profile of 60 keV Al into 4H-SiC crystals," *J. Appl. Phys.*, vol. 93, no. 11, pp. 8914–8917, 2003.

[4] M. S. Janson, M. K. Linnarsson, A. Hallén, and B. G. Svensson, "Electronic stopping cross sections in silicon carbide for low-velocity ions with $1 \leq Z_1 \leq 15$," *J. Appl. Phys.*, vol. 96, no. 1, pp. 164–169, 2004.

[5] S. Tian, "Monte Carlo simulation of ion implantation in crystalline SiC with arbitrary polytypes," *IEEE Trans. Electron Dev.*, vol. 55, no. 8, pp. 1991–1996, 2008.

[6] G. Hobler, "Monte Carlo simulation of two-dimensional implanted dopant distributions at mask edges," *Nucl. Instrum. Meth.*, vol. B 96, pp. 155–162, 1995.

[7] Z. Zolnai, A. Ster, N. Q. Khanh, G. Battistig, T. Lohner, J. Gyulai, E. Kotai, and M. Posselt, "Damage accumulation in nitrogen implanted 6H-SiC: Dependence on the direction of ion incidence and on the ion fluence," *J. Appl. Phys.*, vol. 101, p. 023502, 2007.

[8] J. F. Ziegler, J. P. Biersack, and U. Littmark, *The Stopping and Range of Ions in Solids*. Pergamon Press, New York, 1985.

[9] J. Lindhard and M. Scharff, "Energy Dissipation by Ions in the keV Region," *Phys. Rev.*, vol. 124, no. 1, pp. 128–130, 1961.

[10] K. Nordlund, "Molecular dynamics simulation of ion ranges in the 1–100 keV energy range," *Comp. Mater. Sci.*, vol. 3, pp. 448–456, 1995.